

SCIENTIFIC REPORTS

OPEN

Irradiation-induced β to α SiC transformation at low temperature

Chad M. Parish¹, Takaaki Koyanagi¹, Sosuke Kondo² & Yutai Katoh¹

We observed that β -SiC, neutron irradiated to 9 dpa (displacements per atom) at $\approx 1440^\circ\text{C}$, began transforming to α -SiC, with radiation-induced Frank dislocation loops serving as the apparent nucleation sites. 1440°C is a far lower temperature than usual $\beta \rightarrow \alpha$ phase transformations in SiC. SiC is considered for applications in advanced nuclear systems, as well as for electronic or spintronic applications requiring ion irradiation processing. β -SiC, preferred for nuclear applications, is metastable and undergoes a phase transformation at high temperatures (typically 2000°C and above). Nuclear reactor concepts are not expected to reach the very high temperatures for thermal transformation. However, our results indicate incipient $\beta \rightarrow \alpha$ phase transformation, in the form of small ($\sim 5\text{--}10\text{ nm}$) pockets of α -SiC forming in the β matrix. In service transformation could degrade structural stability and fuel integrity for SiC-based materials operated in this regime. However, engineering this transformation deliberately using ion irradiation could enable new electronic applications.

SiC is a major contender for future applications in advanced nuclear energy systems^{1–3}, as well as for electronic or spintronic applications requiring ion irradiation processing⁴. The β -variant (3C) of SiC is preferred for structural (and many other) applications due to its isotropy, but β -SiC is metastable⁵ and undergoes a phase transformation at high temperatures (typically 2000°C and above) to hexagonal or rhombic SiC, collectively called α -SiC, most often 4H or 6H polytype⁶. Nuclear fission and fusion concepts envision using SiC in applications such as fission-product barriers in fuel kernels⁷, in cladding for accident-tolerant light-water reactor fuels⁸, and in fusion blanket concepts⁹. β -SiC is well known for excellent radiation tolerance^{10,11}. SiC is a nearly ideal material for extreme-environment applications primarily due its inherently irradiation-tolerant matrix¹², but also due to a combination of high-temperature strength and creep resistance and resistance to corrosion from harsh coolants such as Pb-Li. The main disadvantage of SiC is its brittleness, but proper composite design of SiC matrix/SiC fiber composites allows for the amelioration of this brittleness⁹; indeed, SiC/SiC matrix turbine hot-section components is going to be commercialized into jet engines for commercial passenger service. SiC/SiC composites retain good mechanical strength and fracture resistance under many irradiation conditions^{13–15}. Composites and liquid-phase sintered SiC are both strong candidates for accident-tolerant light-water reactor fuel cladding or matrices^{9,16,17}, as a response to the detrimental properties of the present zirconium-alloy fuels demonstrated by the Fukushima disaster, although hydrothermal corrosion may be a limiting factor^{18–22}. SiC is also an important high-temperature/high-power semiconductor^{4,23}, and ion implantation (and its associated damage) is important for device fabrication.

Of SiC's >100 known polytypes, the cubic 3C β -SiC polytype is the main choice for structural and nuclear applications^{24,25}, primarily because of lower processing temperatures and higher isotropy (especially irradiation swelling isotropy) compared to the hexagonal or rhombic α -SiC phases. Transformation by thermal annealing of β to α phase SiC has been studied extensively, and is generally found to occur by slow migration of $\{111\}_\beta \parallel \{0001\}_\alpha$ boundaries with fast migration along directions perpendicular to $\langle 0001 \rangle$ ^{26–28}, and progresses only at temperatures in excess of about 1800°C , and rapidly only above $\sim 2000^\circ\text{C}$. A single observation of lower-temperature $\alpha \rightarrow \beta$ was reported²⁹, with no details. In a predominantly α -phase SiC material, reaction bonded with a small fraction of β -SiC and containing excess Si, the transformation of $\beta \rightarrow \alpha$ was observed under neutron irradiation and post-irradiation annealing^{30,31} ($T_{\text{irrad}} \approx 150^\circ\text{C}$, $T_{\text{anneal}} \approx 1200^\circ\text{C}$), but reports of low-temperature ($<1800^\circ\text{C}$) $\beta \rightarrow \alpha$ transformation in high-purity nuclear-grade β -SiC appear lacking.

In the present study, we irradiated high-purity 3C β -SiC, grown by chemical vapor deposition, in the mixed-spectrum High Flux Isotope Reactor (HFIR) with an average irradiation temperature of $1438 \pm 100^\circ\text{C}$, to a dose of 9 dpa. Previous characterization showed the starting (unirradiated) material contained no α -SiC

¹Oak Ridge National Laboratory, Oak Ridge, TN, 37831, USA. ²Institute of Advanced Energy, Kyoto University, Uji, Kyoto, 611-0011, Japan. Correspondence and requests for materials should be addressed to C.M.P. (email: parishcm@ornl.gov)

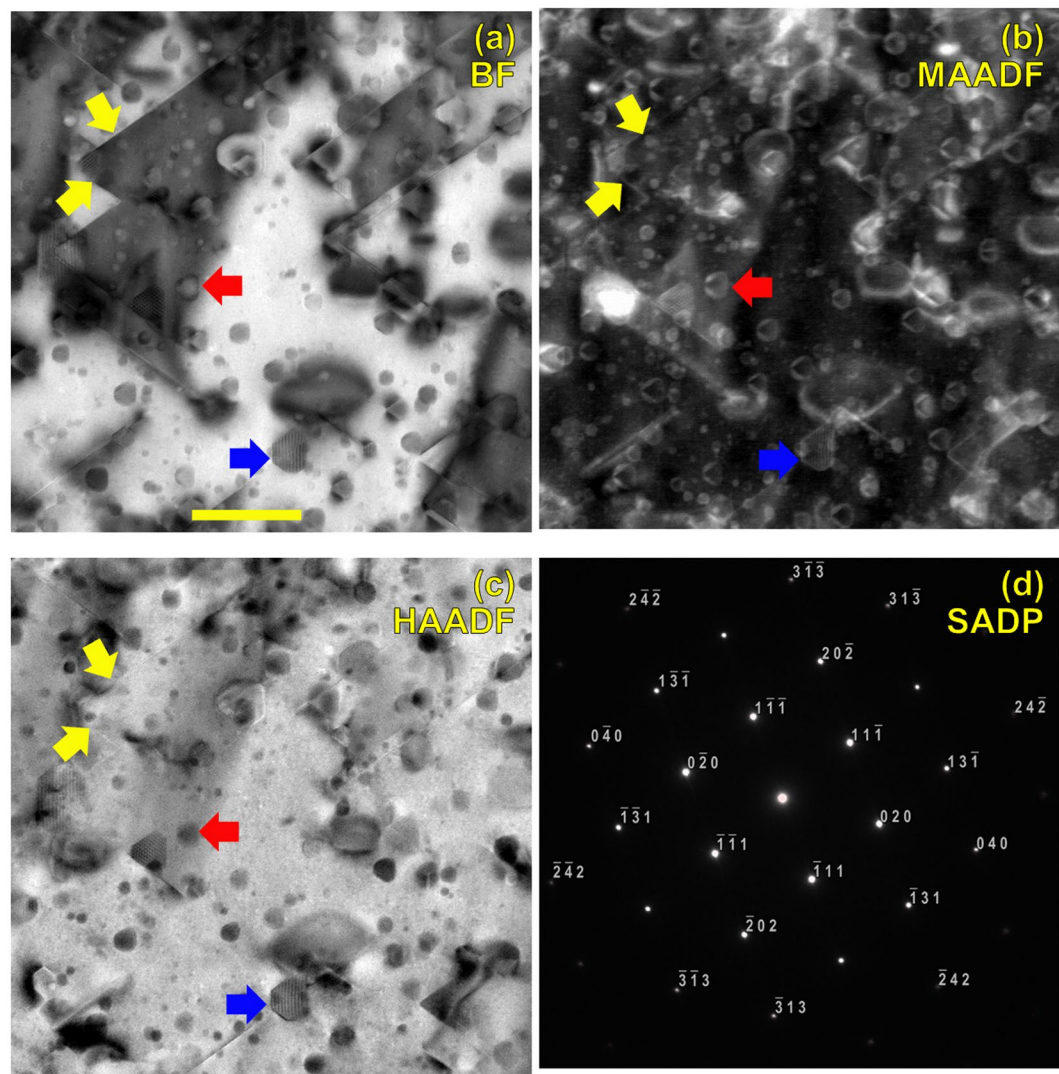


Figure 1. (a) Bright field, (b) medium-angle annular dark-field, and (c) high-angle annular dark field STEM images on the [101] zone axis. (d) Selected-area diffraction pattern. Yellow arrows denote 11-1 and -111 Frank loops. Red arrows denote a tetragonal void with strong diffraction contrast. Blue arrow denotes a region of second-phase material. Scale bar: 50 nm.

phase³². Transmission electron microscopy (TEM), scanning TEM (STEM), and high-resolution transmission electron microscopy (HRTEM) studies of the post-irradiated material were performed to determine what features had evolved; our 1440 °C is among the highest temperature irradiations performed on high-purity β -SiC, and was intended to allow further insight to the temperature/fluence damage mechanism map (e.g., ref. 24, Fig. 17). By using higher-purity starting material and a state-of-the-art S/TEM instrument, we intended to determine if the mechanism maps were accurate in this relatively unexplored region. Based on the published mechanism maps, at 1440 °C, 9 dpa, we expected to see voids^{33,34}, faulted Frank loops on {111} planes²², and possibly unfaulted loops or the early formation of a dislocation network.

Results

The microstructure after irradiation consists of Frank (faulted) loops on {111} planes (Fig. 1, yellow arrows), tetragonal voids (Fig. 1, red arrow), and small (~5–10 nm) regions that showed contrast inconsistent with the expected microstructural features (Fig. 1, blue arrow). These small regions were not expected from published mechanism maps. These unexpected features were seen to be present in several different shapes, with sizes ~5–10 nm, and nearly all of these features were found to be associated with at least one Frank loop (Fig. 2). Out of the nine pockets of anomalous contrast shown in Fig. 2, eight appear to be in contact with a Frank loop (blue \Rightarrow arrows) and one does not appear to be in contact with a Frank loop (yellow \Leftarrow arrow).

Detailed examination of these features indicate that they are α -SiC phase pockets inside the radiation-damaged β -SiC matrix. Regions of matrix and precipitate are marked in Fig. 3(a), and Fourier transforms of these regions are shown in Fig. 3(b,c). The region of 3(b) indexes as cubic β -SiC, on the [101] zone axis, and the Frank loops are

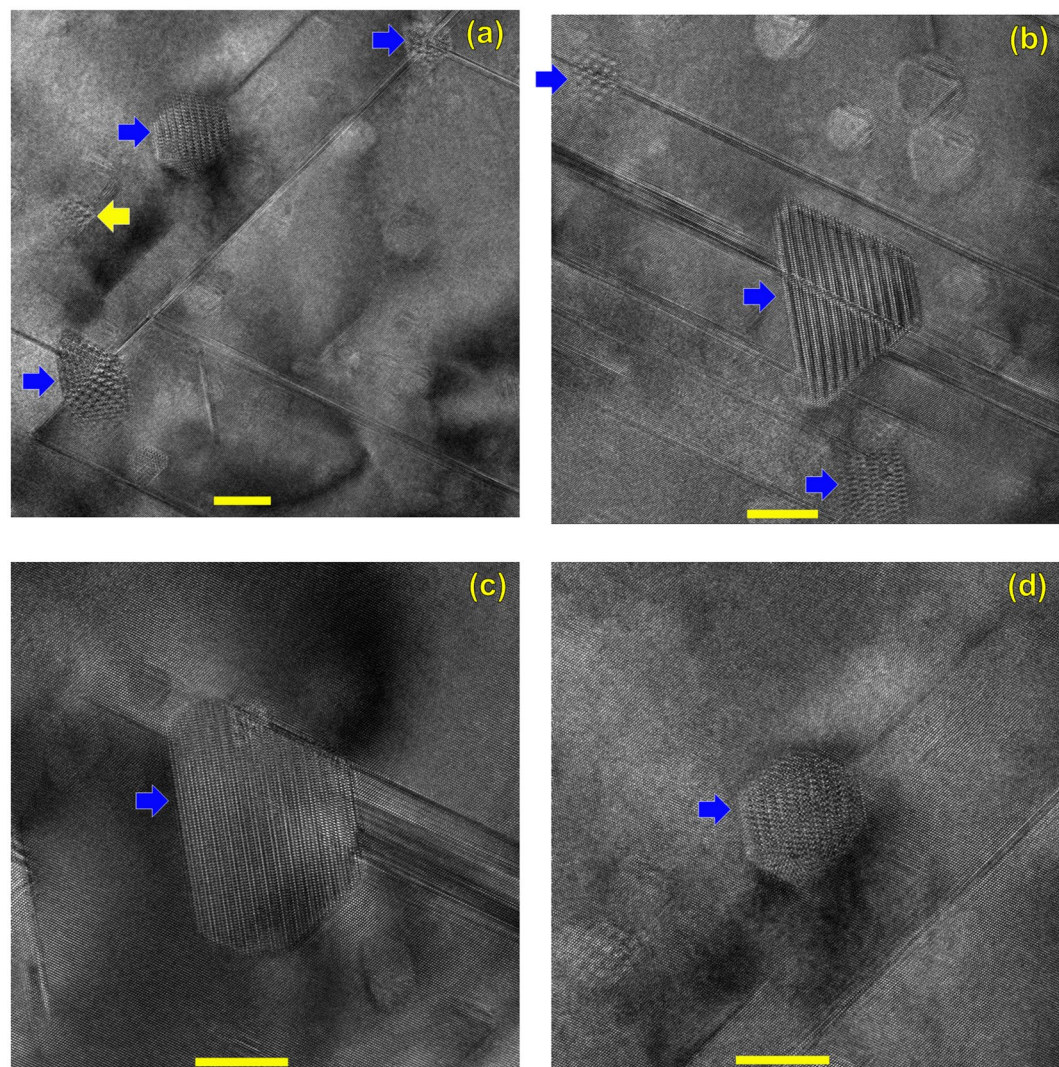


Figure 2. HRTEM images on the [101] zone. Several apparent second-phase precipitates, arrowed, are present. Most or all of these precipitates are located adjacent to a Frank loop (blue \Rightarrow arrows), and one appears not to be adjacent to a Frank loop (yellow \Leftarrow arrow). All scale bars 10 nm.

seen to lie on the $\pm(11\bar{1})$ and $\pm(\bar{1}\bar{1}1)$ planes. The pocket of second phase indexes as the 6H variant of α -SiC, Fig. 3(c), and the [0006] direction of the 6H phase is aligned perfectly with the $[\bar{1}\bar{1}1]$ direction of the cubic matrix; because the lattice plane spacings $d_{(111)}$ of β -SiC and d_{0006} of 6H α -SiC are both 0.252 nm, this orientation relationship is expected. A Fourier transform of the entire micrograph (Fig. 3(d)) shows the expected complexity: bright β -SiC spots, weak α -SiC spots, and streaking associated with the Frank loops. Filtering out the β -SiC reflections and inverse transformation yields Fig. 3(e), which shows the β -SiC matrix removed and only the defects, such as the α pocket and the Frank loops, remaining.

Not all of the α -SiC pockets show the perfect $\langle 111 \rangle_{\beta} \parallel \langle 000 \ell \rangle_{\alpha}$ orientation relationship, Fig. 4. Fourier transforms of matrix and second-phase pocket from Fig. 4(a) are shown in Fig. 4(b,c). The β -SiC matrix indexes identically as before. However, the α -like diffractogram is rotated such that the basal direction is parallel to the $\langle 020 \rangle_{\beta}$ direction of the matrix, which is unexpected. Although a 6H pattern is superimposed on the diffractogram in the bottom of Fig. 4(c), this is not an exact match. The point-to-point spacing in each of the $\{000\ell\}$ zones is $\sim 0.6 \text{ nm}^{-1}$ (or real-space spacing $\sim 1.6 \text{ nm}$), which is near but not exactly the 6H c-direction lattice parameter. By finding the calibration ($\text{nm}^{-1}/\text{pixel}$) for the diffractograms from the β -SiC pattern in panel (b), the same magnification can be applied to the 6H pattern superimposed in panel (c). The simulated zones such as $(0\bar{1}1\ell)$ and $(0\bar{1}\bar{1}\ell)$ in Fig. 4(c) are seen to lie outside the experimental zones, indicating a possible lattice expansion. Regardless, the lack of an exact match is probably due to either strain imposed by not lining up with the easy $\langle 111 \rangle_{\beta} \parallel \langle 000 \ell \rangle_{\alpha}$ direction, and/or the α pocket is not necessarily a single-polytype region. (Transformation to multiple α phases is observed during thermal $\beta \rightarrow \alpha$ transformation resulting in, essentially, “one dimensional disorder” along $\langle 0001 \rangle^{35}$). The entire image Fig. 4(a) was Fourier transformed, filtered to remove β -SiC, and inverse transformed, showing only the Frank loops and second phase particles, Fig. 4(d,e).

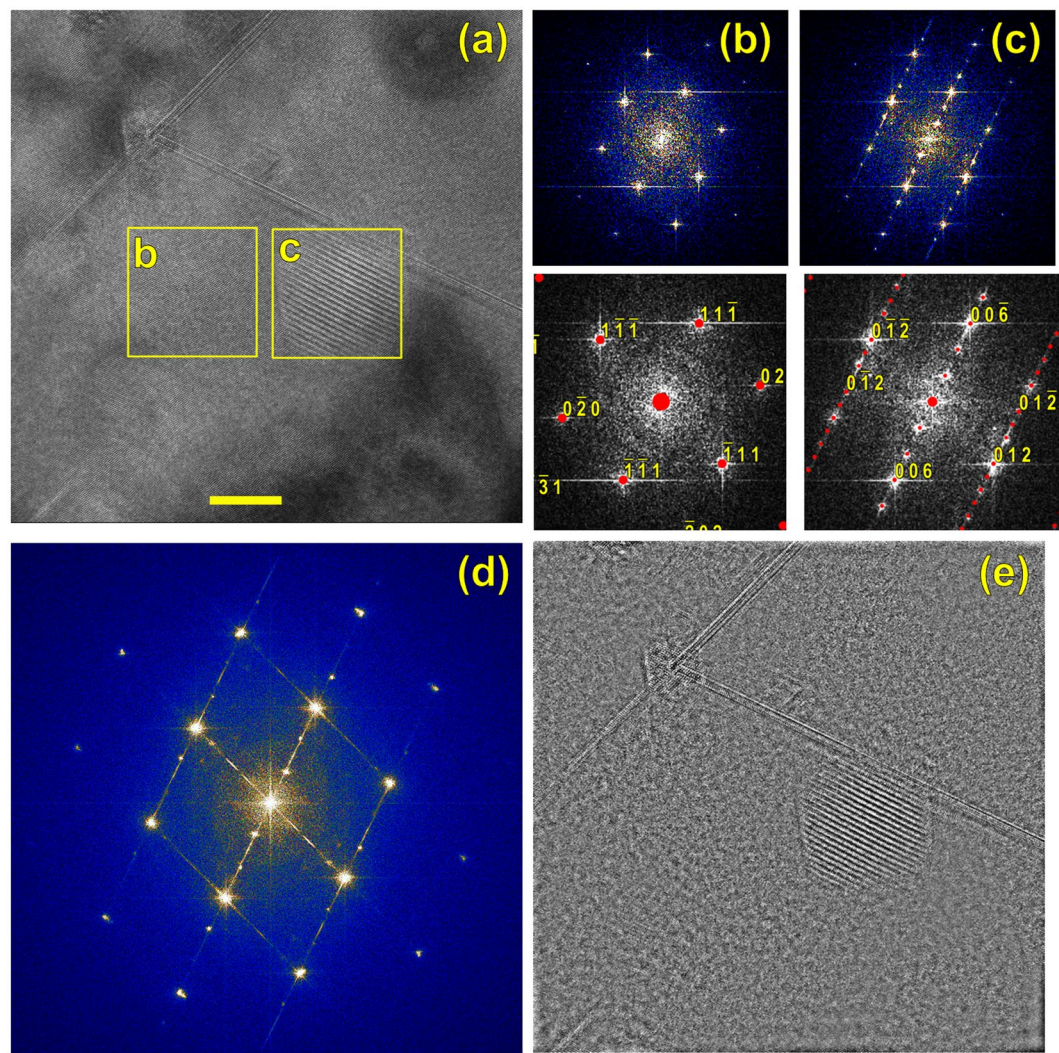


Figure 3. HRTEM image on the $[101]$ matrix zone. Boxes marked “b” and “c” denote the Fourier transforms of (b) and (c), which also show calculated diffraction patterns for 3C and 6H SiC. (d) The Fourier transform of the entire image, showing dislocation streaks, cubic spots, and precipitate spots. (e) Inverse Fourier transform after the cubic spots were removed from (d); only the precipitates and dislocations remain. Scale bar 10 nm.

Pockets of α with $\langle 101 \rangle_{\beta} \parallel \langle 0001 \rangle_{\alpha}$ were also observed. The matrix and α -pocket regions marked in Fig. 5(a) were Fourier transformed into Fig. 5(b,c). Again, the matrix indexes as clean $\langle 101 \rangle_{\beta}$. A more hexagonal or hexagon-like pattern is found for the second-phase pocket, Fig. 5(c). The pattern does not index satisfactorily as, for instance, $\langle 0001 \rangle$ -oriented 6H α -SiC (bottom half, Fig. 5(c)). Likely, a double-diffraction condition is occurring in which the α -phase is near the exit surface of the foil, and strong β reflections are causing the moiré-like effects seen in the image. Supplemental Figure S1 shows a double-diffraction simulation where 6H $\langle 0001 \rangle$ patterns are centered with the origins on each of the strong β $\langle 101 \rangle$ reflections; the match is imperfect but quite close. We therefore conclude that Fig. 5 shows an α -SiC precipitate oriented with $\langle 101 \rangle_{\beta} \parallel \langle 0001 \rangle_{\alpha}$, although the exact α -polytype cannot be discerned, because all $\langle 0001 \rangle_{\alpha}$ -SiC diffraction patterns are very similar, showing a hexagon. The 2H, 4H, 6H, 8H, etc. all show the same spacing in the hexagonal pattern, as well. The overall diffractogram (Fig. 5(d)) shows the expected features and filtering and inverse transformation leaves only the Frank loops and α pocket, Fig. 5(e).

Discussion

As illustrated above, we have observed the incipient conversion of high-purity β -SiC into α -SiC, under neutron irradiation, at temperatures (~ 1440 °C) far below temperatures needed for the thermal conversion of $\beta \rightarrow \alpha$ SiC. We have also noted that almost all of the observed pockets of α phase (Fig. 2) are associated with a Frank loop. Because of the nature of TEM, that is, a two-dimensional projection of a three-dimensional thin foil, we cannot say unequivocally that the α pockets were in intimate contact with the Frank loops. (Similarly, the small number of non-Frank-loop associated α could have formed on loops that were milled off during thin foil preparation). However, because the Frank loops are essentially a confined region of α -phase (a stacking fault), and stacking

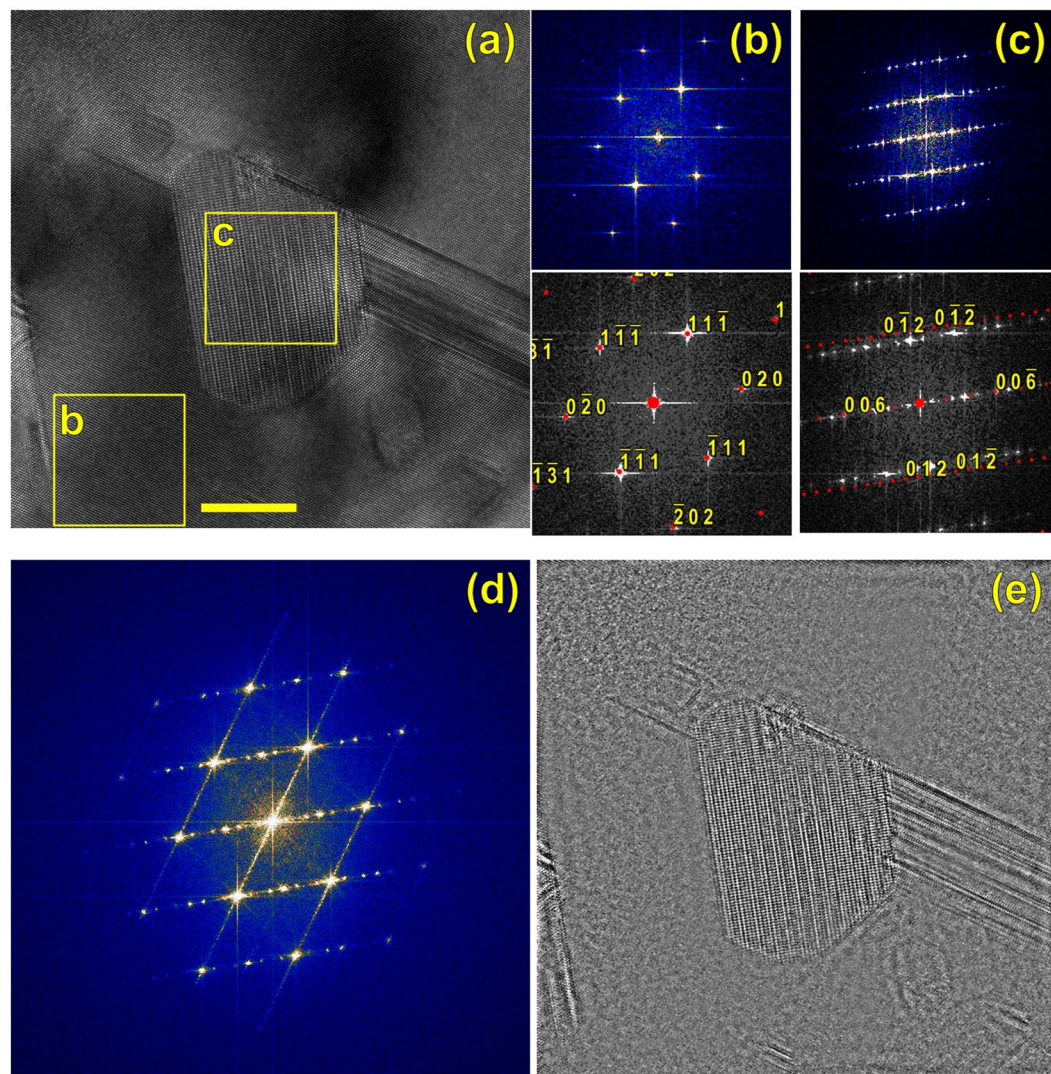


Figure 4. HRTEM image on the [101] matrix zone. Boxes marked “b” and “c” denotes the Fourier transforms of (b) and (c), which also show calculated diffraction patterns for 3C and 6H SiC. (The 6H pattern is not an exact match). (d) The Fourier transform of the entire image, showing dislocation streaks, cubic spots, and precipitate spots. (e) Inverse Fourier transform after the cubic spots were removed from (d); only the precipitates and dislocations remain. Scale bar 10 nm.

faults nucleate the thermal $\beta \rightarrow \alpha$ transformation²⁶, we hypothesize that these irradiation-induced Frank loops serve as pre-existing nucleation sites for the α pocket formation in this situation, and reducing the nucleation barrier. Because faulted loops are generally not present in unirradiated material, we can hypothesize they are assisting the $\beta \rightarrow \alpha$ transition at lower temperature. However, faulted loops have also been observed in lower temperature SiC irradiations that did not show $\beta \rightarrow \alpha$ conversion, so it appears that faulted loops are a necessary but not sufficient condition.

This process appears fundamentally different from some previously observed phenomena in irradiated materials. For instance, growth of second phases in zircon, hafnon, and thorite were observed to occur from the melt zone of a displacement cascade³⁶. However, SiC is not believed to produce large clusters from cascades or suffer a thermal-spike melt³⁷, so a different mechanism is probably present in SiC compared to zircon, hafnon, and thorite. The graphite to diamond irradiation-induced transformation has also been observed^{38,39}, and attributed to a reduced effective free energy difference under irradiation. Given the small energy difference between SiC polytypes under equilibrium conditions, a reduced effective free energy difference during irradiation seems likely. It is possible that the local increase in point-defect density or the increased local energy state assists growth from the Frank loop edge, using a Frank loop as an α nuclei, to form a region of α phase.

Here we compare, very roughly, thermal diffusion to radiation-enhanced diffusion. A few hours at 2000 °C can transform a large fraction of β -SiC to α -SiC^{6,28}, with corresponding diffusion lengths L (calculated as $\sqrt{(Dt)}$ for diffusion coefficient D ^{33,34} and time t) of $L_C \approx 2000$ nm and $L_{Si} \approx 200$ nm. At 1440 °C for $t = 9 \times 10^6$ sec (the approximate in-reactor temperature and time), thermal diffusion would produce $L_C \approx 60$ nm and $L_{Si} \approx 3$ nm.

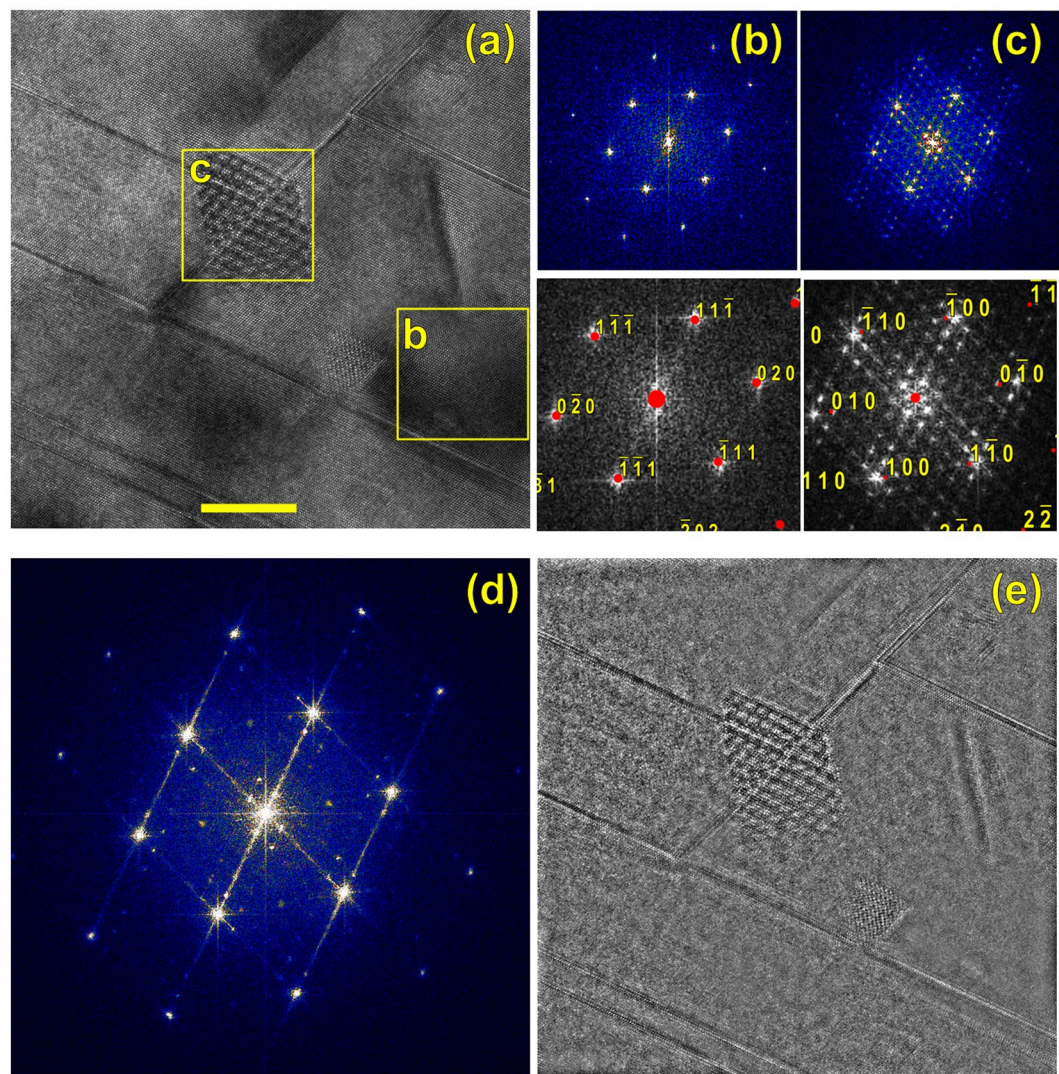


Figure 5. HRTEM image on the [101] matrix zone. Boxes marked “b” and “c” denotes the Fourier transforms of (b) and (c), which also show calculated diffraction patterns for 3C and 6H SiC. (d) The Fourier transform of the entire image, showing dislocation streaks, cubic spots, and precipitate spots. (e) Inverse Fourier transform after the cubic spots were removed from (d); only the precipitates and dislocations remain. Scale bar 10 nm.

Using the SiC radiation enhanced self-diffusion coefficients and point-defect concentrations from ref. 40, we estimate $L_C^{RE} \sim 300$ nm and $L_{Si}^{RE} \sim 100$ nm at 1440 °C for 9×10^6 sec. Although L_C^{RE} and L_{Si}^{RE} numbers are approximate, these radiation-enhanced self-diffusion lengths are roughly comparable to higher temperature thermal conditions that produce partial b to a transformation, suggesting that increased diffusivity arising from radiation-induced point defects allows the transformation to occur in observable periods at lower temperatures observed in this work. This leads to the important hypothesis that higher damage rates, obtainable with ion or electron accelerators, could drive this β to α transformation more quickly and be used in an industrial or microelectronic application.

Polytype nanostructuring of SiC is an emerging field for future electronics and spintronics (for instance, refs 4, 41 and 42). If the presently observed low-temperature phase transformation can be induced via high-energy ion or electron irradiation (which can both produce displacement damage broadly similar to neutrons) then the control of the transformation may potentially be engineered for electronic or spintronic applications.

In summary, we report the conversion of high-purity β -SiC to α -SiC at surprisingly low temperature (~ 1440 °C) under mixed-spectrum neutron irradiation to ~ 9 dpa. 6H polytype α -SiC has been unambiguously identified, and other polytypes may be present. Both the expected $\langle 111 \rangle_\beta \| \langle 000 \rangle_\alpha$ orientation, and unexpected orientations, e.g., $\langle 020 \rangle_\beta \| \langle 000 \rangle_\alpha$ and $\langle 101 \rangle_\beta \| \langle 000 \rangle_\alpha$ have been observed. Regardless of the mechanism, the observation of the $\beta \rightarrow \alpha$ conversion in SiC under irradiation may have significant implications for in-service behavior, due to changes in isotropy and increases in boundary surface area that could affect diffusion of fission products⁴³. For instance, in TRISO fission fuel, CVD β -SiC serves as a barrier to fission product, fission gas, and actinide escape. Under certain conditions (e.g., refs 44 and 45) the SiC layer in TRISO could experience

doses and temperatures similar to those in this study, and conversion of $\beta \rightarrow \alpha$ SiC would have effects on the containment of radioisotopes presently not understood or accounted for in TRISO models. Further, under accident conditions, the SiC – which would contain copious Frank loops – would be subjected to high temperatures (perhaps 1700 or 1800 °C), and the pre-existing Frank loops might serve as excellent nucleation sites for the thermal conversion of $\beta \rightarrow \alpha$ SiC during the loss-of-coolant temperature excursion. In short, the $\beta \rightarrow \alpha$ SiC conversion will have implications for future nuclear applications, and needs to be studied and modelled in detail. Further, different polymorphs can be used in electronic or spintronic engineering⁴, and therefore introduction of these domains in a controlled manner using ions or electrons (rather than neutrons) may lead to new semiconductor or optoelectronic applications.

Methods

The 3C-SiC samples were chemical vapor deposition samples from Rohm and Haas Advanced Materials (presently Dow Chemical, Woburn, MA). Samples were in the form of disks of size 6 mm diameter and 0.5 or 3.2 mm in thickness. They were irradiated to a fluence of 9.6×10^{25} n/m², about 9–10 dpa, in the ORNL High Flux Isotope Reactor, in the METS irradiation campaign. Thermometry indicated an irradiation temperature of approximately 1438 ± 100 °C. ±100 °C is a pessimistic bound based on melt wires; we estimate ±25 °C is more likely in reality, based on experience from other irradiation campaigns. Dose rate was $\sim 1 \times 10^{-6}$ dpa/sec.

Samples were prepared by extracting the disks from the irradiation capsules in the ORNL hot cells, shipping them to our hands-on irradiated materials lab (LAMDA)⁴⁶, cleaning, grinding, polishing, and mounting for focused ion beam (FIB) preparation, all in a radiological contamination zone. The samples were then moved from the radiological contamination zone to the clean suite of our laboratory, and imaged in an FEI Versa DualBeam FIB-SEM (scanning electron microscope) tool. Electron backscatter diffraction was used to find grains oriented near $\langle 101 \rangle$ in-plane, which were prepared for TEM using the FIB system. Samples were cleaned down to 2 kV Ga⁺ in the Versa DualBeam system, and then were transferred to a Fishione Nanomill system and milled with 900 eV and 600 eV Ar⁺ at ±10° off glancing incidence. This Ar⁺ post-FIB cleaning removes essentially all FIB damage in SiC. By performing the Ar⁺ cleaning less than five minutes prior to loading the samples into the TEM, the possibility of oxidation or anomalous oxide contrast is minimized or eliminated.

TEM and STEM were performed in an FEI Talos F200X tool⁴⁷, operated at 200 keV. Both STEM and TEM were performed with 3C-SiC grains on the $\langle 101 \rangle$ orientation. STEM images were acquired in high-angle annular dark field, medium angle annular dark field, and bright field modes. Estimated STEM detector collection angles were: HAADF, 77–200 mrad; MAADF, 18–77 mrad; BF, 0–10 mrad. TEM images were acquired with a large objective aperture, using the 4096 × 4096 pixel TEM camera (FEI Ceta) mounted to the Talos tool. Post processing used Gatan Digital Micrograph software. The double diffraction pattern (Supplemental Figure S1) was produced by simulating 3C and 6H patterns in CrystalMaker™ software, importing the simulated diffraction patterns and the experimental Fourier transform into PhotoShop™ software, applying transparency to the simulated diffraction patterns, and using each major reflection in the 3C pattern as an origin for a copy of the 6H pattern.

References

- Zinkle, S. J. & Busby, J. T. Structural materials for fission & fusion energy. *Mater. Today* **12**, 12–19 (2009).
- Zinkle, S. J. & Was, G. S. Materials challenges in nuclear energy. *Acta Materialia* **61**, 735–758, doi:10.1016/j.actamat.2012.11.004 (2013).
- Zhang, Y. *et al.* Ionization-induced annealing of pre-existing defects in silicon carbide. *Nat Commun* **6**, doi:10.1038/ncomms9049 (2015).
- Falk, A. L. *et al.* Polytype control of spin qubits in silicon carbide. *Nat Commun* **4**, 1819, doi:10.1038/ncomms2854 (2013).
- Limpijumnong, S. & Lambrecht, W. R. L. Total energy differences between SiC polytypes revisited. *Physical Review B* **57**, 12017 (1998).
- Bind, J.-M. Phase transformation during hot-pressing of cubic SiC. *Materials Research Bulletin* **13**, 91–96 (1978).
- Minato, K. *et al.* Fission product behavior in Triso-coated UO₂ fuel particles. *Journal of Nuclear Materials* **208**, 266–281 (1994).
- Zinkle, S. J., Terrani, K. A., Gehin, J. C., Ott, L. J. & Snead, L. L. Accident tolerant fuels for LWRs: A perspective. *Journal of Nuclear Materials* **448**, 374–379 (2014).
- Katoh, Y., Snead, L. L., Szlufarska, I. & Weber, W. J. Radiation effects in SiC for nuclear structural applications. *Current Opinion in Solid State and Materials Science* **16**, 143–152 (2012).
- Jiang, M. *et al.* Ab initio molecular dynamics simulation of the effects of stacking faults on the radiation response of 3C-SiC. *Scientific reports* **6** (2016).
- Chen, D., Gao, F. & Liu, B. Grain boundary resistance to amorphization of nanocrystalline silicon carbide. *Scientific reports* **5** (2015).
- Zinkle, S. J. & Snead, L. L. Designing Radiation Resistance in Materials for Fusion Energy. *Annual Review of Materials Research* **44**, 241–267, doi:10.1146/annurev-matsci-070813-113627 (2014).
- Katoh, Y. *et al.* High-dose neutron irradiation of Hi-Nicalon Type S silicon carbide composites. Part 2: Mechanical and physical properties. *Journal of Nuclear Materials* **462**, 450–457 (2015).
- Katoh, Y. *et al.* Current status and recent research achievements in SiC/SiC composites. *Journal of Nuclear Materials* **455**, 387–397 (2014).
- Perez-Bergquist, A. G. *et al.* High dose neutron irradiation of Hi-Nicalon Type S silicon carbide composites, Part 1: Microstructural evaluations. *Journal of Nuclear Materials* **462**, 443–449 (2015).
- Kim, D., Lee, H.-G., Park, J. Y. & Kim, W.-J. Fabrication and measurement of hoop strength of SiC triplex tube for nuclear fuel cladding applications. *Journal of Nuclear Materials* **458**, 29–36 (2015).
- Besmann, T. M., Ferber, M. K., Lin, H.-T. & Collin, B. Fission product release and survivability of UN-kernel LWR TRISO fuel. *Journal of Nuclear Materials* **448**, 412–419 (2014).
- Terrani, K. A. *et al.* Hydrothermal corrosion of SiC in LWR coolant environments in the absence of irradiation. *Journal of Nuclear Materials* **465**, 488–498 (2015).
- Kondo, S., Lee, M., Hinoki, T., Hyodo, Y. & Kano, F. Effect of irradiation damage on hydrothermal corrosion of SiC. *Journal of Nuclear Materials* **464**, 36–42 (2015).

20. Tan, L., Allen, T. R. & Barringer, E. Effect of microstructure on the corrosion of CVD-SiC exposed to supercritical water. *Journal of Nuclear Materials* **394**, 95–101, doi:10.1016/j.jnucmat.2009.08.008 (2009).
21. Parish, C. M., Terrani, K. A., Kim, Y.-J., Koyanagi, T. & Katoh, Y. Microstructure and hydrothermal corrosion behavior of NITE-SiC with various sintering additives in LWR coolant environments. *Journal of the European Ceramic Society* **37**, 1261–1279, doi:10.1016/j.jeurceramsoc.2016.11.033 (2017).
22. Kondo, S., Mouri, S., Hyodo, Y., Hinoki, T. & Kano, F. Role of irradiation-induced defects on SiC dissolution in hot water. *Corrosion Science* **112**, 402–407 (2016).
23. Osterberg, D. D., Youngsman, J., Ubic, R., Reimanis, I. E. & Butt, D. P. Recrystallization Kinetics of 3C Silicon Carbide Implanted with 400 keV Cesium Ions. *Journal of the American Ceramic Society* **96**, 3290–3295 (2013).
24. Snead, L. L. *et al.* Handbook of SiC properties for fuel performance modeling. *Journal of Nuclear Materials* **371**, 329–377, doi:10.1016/j.jnucmat.2007.05.016 (2007).
25. Katoh, Y. *et al.* Continuous SiC fiber, CVI SiC matrix composites for nuclear applications: Properties and irradiation effects. *Journal of Nuclear Materials* **448**, 448–476, doi:10.1016/j.jnucmat.2013.06.040 (2014).
26. Ogbuji, L. U., Mitchell, T. E. & Heuer, A. H. The beta-alpha transformation in polycrystalline SiC: 3, the thickening of alpha plates. *Journal of the American Ceramic Society* **64**, 91–99, doi:10.1111/j.1151-2916.1981.tb09583.x (1981).
27. Mitchell, T. E., Ogbuji, L. U. & Heuer, A. H. Beta-alpha transformation in polycrystalline SiC: 2, interfacial energetics. *Journal of the American Ceramic Society* **61**, 412–413, doi:10.1111/j.1151-2916.1978.tb09349.x (1978).
28. Heuer, A. H., Fryburg, G. A., Ogbuji, L. U., Mitchell, T. E. & Shinozaki, S. Beta-alpha transformation in polycrystalline SiC: 1, microstructural aspects. *Journal of the American Ceramic Society* **61**, 406–412, doi:10.1111/j.1151-2916.1978.tb09348.x (1978).
29. Powell, J. A. & Will, H. A. Low-Temperature Solid-State Phase Transformations in 2H Silicon Carbide. *Journal of Applied Physics* **43**, 1400–1408 (1972).
30. Harrison, S. & Corelli, J. Microstructure of polycrystalline SiC containing excess Si after neutron and ion irradiation. *Journal of Nuclear Materials* **99**, 203–212 (1981).
31. Harrison, S. & Corelli, J. Microstructure of neutron irradiation-induced defects in sintered and siliconized SiC. *Journal of Nuclear Materials* **122**, 833–839 (1984).
32. Katoh, Y., Snead, L. L., Parish, C. M. & Hinoki, T. Observation and possible mechanism of irradiation induced creep in ceramics. *Journal of Nuclear Materials* **434**, 141–151, doi:10.1016/j.jnucmat.2012.11.035 (2013).
33. Kondo, S., Katoh, Y. & Snead, L. L. Unidirectional formation of tetrahedral voids in irradiated silicon carbide. *Appl. Phys. Lett.* **93**, 163110 (2008).
34. Kondo, S., Katoh, Y. & Snead, L. L. Microstructural defects in SiC neutron irradiated at very high temperatures. *Journal of Nuclear Materials* **382**, 160–169 (2008).
35. Shinozaki, S. & Kinsman, K. R. Aspects of one dimensional disorder in silicon carbide. *Acta Metallurgica* **26**, 769–776, doi:10.1016/0001-6160(78)90027-5 (1978).
36. Meldrum, A., Zinkle, S., Boatner, L. & Ewing, R. C. A transient liquid-like phase in the displacement cascades of zircon, hafnium and thorite. *Nature* **395**, 56–58 (1998).
37. Gao, F. & Weber, W. J. Atomic-scale simulation of 50 keV Si displacement cascades in β -SiC. *Physical Review B* **63**, 054101 (2000).
38. Banhart, F. & Ajayan, P. Carbon onions as nanoscopic pressure cells for diamond formation. *Nature* **382**, 433 (1996).
39. Zaiser, M. & Banhart, F. Radiation-induced transformation of graphite to diamond. *Physical Review Letters* **79**, 3680 (1997).
40. Dwaraknath, S. S. & Was, G. S. Radiation enhanced diffusion of cesium, strontium, and europium in silicon carbide. *Journal of Nuclear Materials* **474**, 76–87, doi:10.1016/j.jnucmat.2016.02.034 (2016).
41. Heremans, F. J., Yale, C. G. & Awschalom, D. D. Control of Spin Defects in Wide-Bandgap Semiconductors for Quantum Technologies. *Proceedings of the IEEE*, doi:10.1109/JPROC.2016.2561274 (in press).
42. Castelletto, S. *et al.* A silicon carbide room-temperature single-photon source. *Nature Materials* **13**, 151–156 (2014).
43. Friedland, E. *et al.* Study of silver diffusion in silicon carbide. *Journal of Nuclear Materials* **389**, 326–331 (2009).
44. Demkowicz, P. A. *et al.* “INL/CON-12-24427: Preliminary results of post-irradiation examination of the AGR-1 TRISO fuel compacts” US Government Publication. <https://inldigitalibrary.inl.gov/sti/5605028.pdf> (2012).
45. US Department of Energy, “INL/EXT-11-22880: Analytical Neutronic Studies Correlating Fast Neutron Fluence to Material Damage in Carbon, Silicon, and Silicon Carbide,” US Government Publication. <https://inldigitalibrary.inl.gov/sti/5029085.pdf> (2011).
46. Parish, C. M. *et al.* LAMDA: Irradiated-Materials Microscopy at Oak Ridge National Laboratory. *Microscopy and Microanalysis* **21**, 1003–1004 (2015).
47. Parish, C. M. MT3FT-15OR0204122: Report on the acquisition and installation of FEI Talos F200X S/TEM. (Oak Ridge National Laboratory (ORNL), Oak Ridge, TN (United States) <http://www.osti.gov/servlets/purl/1234344/>) (2015).

Acknowledgements

This research was supported by the U.S. Department of Energy, Office of Science, Fusion Energy Sciences. This manuscript has been authored by UT-Battelle, LLC, under Contract No. DE-AC05-00OR22725 with the U.S. Department of Energy. This research was performed, in part, using instrumentation provided by the Department of Energy, Office of Nuclear Energy, Fuel Cycle R&D Program and the Nuclear Science User Facilities (FEI Talos F200X S/TEM). Dr. Larry Allard, ORNL, and Dr. Steve Zinkle, University of Tennessee, provided valuable advice. Several images generated using SingleCrystal™: a diffraction program for Mac and Windows. CrystalMaker Software Ltd, Oxford, England (<www.crystallmaker.com>). The ORNL LAMDA lab Radiological Control Technician team made this research possible and helped us work efficiently and safely.

Author Contributions

Y.K. and S.K. designed and performed the irradiation campaign. T.K. performed sample preparation of the radioactive material. C.M.P. performed the electron microscopy and drafted the manuscript. All authors revised and contributed to the final manuscript.

Additional Information

Supplementary information accompanies this paper at doi:10.1038/s41598-017-01395-y

Competing Interests: The authors declare that they have no competing interests.

Publisher's note: Springer Nature remains neutral with regard to jurisdictional claims in published maps and institutional affiliations.



Open Access This article is licensed under a Creative Commons Attribution 4.0 International License, which permits use, sharing, adaptation, distribution and reproduction in any medium or format, as long as you give appropriate credit to the original author(s) and the source, provide a link to the Creative Commons license, and indicate if changes were made. The images or other third party material in this article are included in the article's Creative Commons license, unless indicated otherwise in a credit line to the material. If material is not included in the article's Creative Commons license and your intended use is not permitted by statutory regulation or exceeds the permitted use, you will need to obtain permission directly from the copyright holder. To view a copy of this license, visit <http://creativecommons.org/licenses/by/4.0/>.

© The Author(s) 2017